Temperature-driven transition from the Wigner crystal to the bond-charge-density wave in the quasi-one-dimensional quarter-filled band

R. T. Clay,[1] R. P. Hardikar,[1] and S. Mazumdar[2]
[1]*Department of Physics and Astronomy and HPC*[2] *Center for Computational Sciences, Mississippi State University, Mississippi 39762, USA*
[2]*Department of Physics, University of Arizona, Tucson, Arizona 85721, USA*
(Received 21 September 2007; published 27 November 2007)

It is known that within the interacting electron model Hamiltonian for the one-dimensional $\frac{1}{4}$-filled band, the singlet ground state is a Wigner crystal only if the nearest-neighbor electron-electron repulsion is larger than a critical value. We show that this critical nearest-neighbor Coulomb interaction is different for each spin subspace, with the critical value decreasing with increasing spin. As a consequence, with the lowering of temperature, there can occur a transition from a Wigner crystal charge-ordered state to a spin-Peierls state that is a bond-charge-density wave with charge occupancies different from the Wigner crystal. This transition is possible because spin excitations from the spin-Peierls state in the $\frac{1}{4}$-filled band are necessarily accompanied by changes in site charge densities. We apply our theory to the $\frac{1}{4}$-filled band quasi-one-dimensional organic charge-transfer solids, in general, and to 2:1 tetramethyltetrathiafulvalene (TMTTF) and tetramethyltetraselenafulvalene cationic salts, in particular. We believe that many recent experiments strongly indicate the Wigner crystal to bond-charge-density Wave transition in several members of the TMTTF family. We explain the occurrence of two different antiferromagnetic phases but a single spin-Peierls state in the generic phase diagram for the 2:1 cationic solids. The antiferromagnetic phases can have either the Wigner crystal or the bond-charge-spin-density wave charge occupancies. The spin-Peierls state is always a bond-charge-density wave.

DOI: 10.1103/PhysRevB.76.205118 PACS number(s): 71.30.+h, 71.45.Lr, 74.70.Kn

I. INTRODUCTION

Spatial broken symmetries in the quasi-one-dimensional (quasi-1D) $\frac{1}{4}$-filled organic charge-transfer solids (CTSs) have been of strong experimental[1–17] and theoretical[18–26] interests. The broken symmetry states include charge order (hereafter CO, this is usually accompanied by intramolecular distortions), intermolecular lattice distortions (hereafter bond order wave or BOW), antiferromagnetism (AFM), and spin-Peierls (SP) order. Multiple orderings may compete or even coexist simultaneously. Interestingly, these unconventional insulating states in the CTS are often proximate to superconductivity,[27] the mechanism of which has remained perplexing after intensive investigations over several decades. Unconventional behavior at or near $\frac{1}{4}$ filling has also been observed in the quasi-two-dimensional organic CTS with higher superconducting critical temperatures,[11,28–31] sodium cobaltate,[32–34] and oxides of titanium[35] and vanadium.[36,37]

In spite of extensive research on 1D instabilities in the CTS, detailed comparisons of theory and experiments remain difficult. Strong electron-electron (e-e) Coulomb interactions in these systems make calculations particularly challenging, and with few exceptions[38,39] existing theoretical discussions of broken symmetries in the interacting $\frac{1}{4}$-filled band have been limited to the *ground* state.[18–25] This leaves a number of important questions unresolved, as we point out below.

Quasi-1D CTS undergo two distinct phase transitions as the temperature (hereafter T) is reduced.[40] The $4k_F$ transition at higher T involves charge degrees of freedom ($T_{4k_F} \sim 100$ K), with the semiconducting state below $4k_F$ exhibiting either a dimerized CO or a dimerized BOW. Charges alternate as $0.5+\epsilon$ and $0.5-\epsilon$ on the molecules along the stack in the dimerized CO. The site charge occupancy in the dimerized CO state is commonly written as $\cdots 1010 \cdots$ (with "1" and "0" denoting charge-rich and charge-poor sites), and this state is also referred to as the Wigner crystal. The $4k_F$ BOW has alternating intermolecular bond strengths, but site charges are uniformly 0.5. It is generally accepted that the dimer CO (dimer BOW) is obtained for strong (weak) intermolecular Coulomb interactions (the intramolecular Coulomb interaction can be large in either case, see Sec. III). At $T < T_{2k_F} \sim 10-20$ K, there occurs a second transition in the CTS, involving spin degrees of freedom, to either a SP or an AFM state. Importantly, the SP and the AFM states both can be derived from the dimer CO or the dimer BOW. Coexistence of the SP state with the Wigner crystal would require that the SP state has the structure $1=0=1\cdots 0\cdots 1$, with singlet "bonds" alternating in strength between the charge-rich sites of the Wigner crystal. Similarly, coexisting AFM and Wigner crystal would imply site charge-spin occupancies $\uparrow 0$ $\downarrow 0$. The occurrence of both have been suggested in the literature.[20,26,38,39] The SP state can also be obtained from dimerization of the dimer $4k_F$ BOW, in which case there occurs a spontaneous transition from the uniform charge-density state to a coexisting bond-charge-density wave (BCDW)[18,22,25] $1-1=0\cdots 0$. The unit cells here are dimers with site occupancies 1 and 0 or 0 and 1, with strong and weak interunit 1-1 and $0\cdots 0$ bonds, respectively. The AFM state with the same site occupancies $\cdots 1100 \cdots$ is referred to as the bond-charge-spin-density wave (BCSDW)[21] and is denoted as $\uparrow\downarrow 00$.

The above characterizations of the different states and the related bond, charge and spin patterns are largely based on

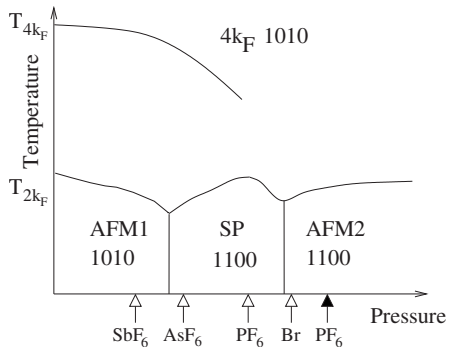

FIG. 1. Schematic of the proposed T versus P phase diagram for $(TMTCF)_2X$, where C=T or S, along with the charge occupancies of the sites in the low T phases as determined in this work. The P axis reflects the extent of interchain coupling. Open (filled) arrows indicate the ambient pressure locations of TMTTF (TMTSF) salts.

ground state calculations. The mechanism of the transition from the $4k_F$ state to the $2k_F$ state lies outside the scope of such theories. Questions that remain unresolved as a consequence include the following: (i) Does the nature of the $4k_F$ state (charge versus bond dimerized) predetermine the site charge occupancies of the $2k_F$ state? This is assumed in many of the published works. (ii) What determines the nature of the $2k_F$ state (AFM versus SP)? (iii) How does one understand the occurrence of two different AFM phases (hereafter AFM1 and AFM2) straddling a single SP phase in the proposed T versus P (where P is pressure) phase diagram (see Fig. 1)[9] for the cationic $\frac{1}{4}$-filled band quasi-1D CTS? (iv) What is the nature of the intermediate T states between the $4k_F$ dimerized state and the $2k_F$ tetramerized state? As we point out in the next section, where we present a brief review of the experimental results, answers to these questions are crucial for a deeper understanding of the underlying physics of the $\frac{1}{4}$-filled band CTS.

In the present paper, we report the results of our calculations of T-dependent behavior within theoretical models incorporating both e-e and electron-phonon (e-p) interactions to answer precisely the above questions. One key result of our work is as follows: in between the strong and weak intermolecular Coulomb interaction parameter regimes, there exists a third parameter regime within which the intermolecular Coulomb interactions are intermediate, and within which there can occur a transition from a Wigner crystal CO state to a BCDW SP state as the T is lowered. Thus the charge or bond ordering in the $4k_F$ phase does *not* necessarily decide the same in the $2k_F$ state. For realistic intramolecular Coulomb interactions (Hubbard U), we show that the width of this intermediate parameter regime is comparable to the strong and weak intersite interaction regimes. We believe that our results are directly applicable to the family of the cationic CTS $CTS(TMTTF)_2X$, where a redistribution of charge upon entering the SP state from the CO state has been observed[15,16] in $X=AsF_6$ and PF_6. A natural explanation of this redistribution emerges within our theory. The SP state within our theory is unique and has the BCDW charge occupancy, while the two AFM regions in the phase diagram of Fig. 1 have different site occupancies. Our theory therefore provides a simple diagnostic to determine the pattern of CO coexisting with low-temperature magnetic states in the $\frac{1}{4}$-filled CTS.

In addition to the above theoretical results directly pertaining to the quasi-1D CTS, our work gives new insight to excitations from a SP ground state in a non-half-filled band. In the case of the usual SP transition within the $\frac{1}{2}$-filled band, the SP state is bond dimerized at $T=0$ and has uniform bonds at $T>T_{2k_F}$. The site charges are uniform at all T. This is in contrast to the $\frac{1}{4}$-filled band, where the SP state at $T=0$ is bond and charge tetramerized and the $T>T_{2k_F}$ state is dimerized as opposed to being uniform. Furthermore, we show that the high T phase here can be either charge or bond dimerized, starting from the same low T state. This clearly requires *two* different kinds of spin excitations in the $\frac{1}{4}$-filled band. We demonstrate that spin excitations from the SP state in the $\frac{1}{4}$-filled band can lead to two different kinds of defects in the background BCDW.

In the next section, we present a brief yet detailed summary of relevant experimental results in the quasi-1D CTS. The scope of this summary makes the need for having T-dependent theory clear. Following this, in Sec. III, we present our theoretical model along with conjectures based on physical intuitive pictures. In Sec. IV, we substantiate these conjectures with accurate quantum Monte Carlo (QMC) and exact diagonalization (ED) numerical calculations. Finally, in Sec. V we compare our theoretical results and experiments, and present our conclusions.

II. REVIEW OF EXPERIMENTAL RESULTS

Examples of both CO and BOW broken symmetries at $T<T_{4k_F}$ are found in the $\frac{1}{4}$-filled CTS. The $4k_F$ phase in the anionic 1:2 CTS is commonly bond dimerized. The most well known example is $MEM(TCNQ)_2$, which undergoes a metal-insulator transition accompanied with bond dimerization at 335 K.[41] Site charges are uniform in this $4k_F$ phase. The $2k_F$ phase in the TCNQ-based systems is universally SP and not AFM. The SP transition in $MEM(TCNQ)_2$ occurs below $T_{2k_F}=19$ K, and low T neutron diffraction measurements of deuterated samples[41] have established that the bond tetramerization is accompanied by $2k_F$ CO$\cdots$1100$\cdots$. X-ray[42,43] and neutron diffraction[44] experiments have confirmed a similar low T phase in $TEA(TCNQ)_2$. We will not discuss these further in the present paper, as they are well described within our previous work.[18,25] We will, however, argue that the SP ground state in $(DMe\text{-}DCNQI)_2Ag$ (Ref. 45) (as opposed to AFM) indicates $\cdots$1100$\cdots$ CO in this.

The cationic $(TMTCF)_2X$, C=S and Se, exhibit more variety, presumably because the counterions affect packing as well as site energies in the cation stack. Differences between systems with centrosymmetric and noncentrosymmetric anions are also observed. Their overall behavior is summarized in Fig. 1, where, as is customary, pressure P can also imply larger interchain coupling. We have indicated schematically the possible locations of different materials on the phase diagram. The most significant aspect of the phase diagram is the occurrence of two distinct antiferromagnetic phases, AFM1 and AFM2, straddling a single SP phase.

Most TMTTF lie near the low P region of the phase diagram and are insulating already at or near room temperature because of charge localization, which is due to the intrinsic dimerization along the cationic stacks.[1,4,11] CO at intermediate temperatures T_{CO} has been found in dielectric permittivity,[4] NMR,[7] and ESR[46] experiments on materials near the low and intermediate P end. Although the pattern of the CO has not been determined directly, the observation of ferroelectric behavior below T_{CO} is consistent with $\cdots 1010 \cdots$ type CO in this region.[5,23] With further lowering of T, most $(TMTTF)_2X$ undergo transitions to the AFM1 or SP phase (with $X=$Br a possible exception, see below). $X=SbF_6$ at low T lies in the AFM1 region,[9] with a very high T_{CO} and relatively low Néel temperature $T_N=8$ K. As the schematic phase diagram indicates, pressure suppresses both T_{CO} and T_N in this region. For $P>0.5$ GPa, $(TMTTF)_2SbF_6$ undergoes a transition from the AFM1 to the SP phase,[9] the details of which are not completely understood; any charge disproportionation in the SP phase is small.[9] $(TMTTF)_2ReO_4$ also has a relatively high $T_{CO}=225$ K, but the low T phase here reached following an anion-ordering transition is spin singlet.[14] Nakamura *et al.* have suggested, based on NMR experiments, that the CO involves the Wigner crystal state, but the low T state is the $\cdots 1100 \cdots$ BCDW.[14] Further along the P axis lie $X=AsF_6$ and PF_6, where T_{CO} are reduced to 100 K and 65 K, respectively.[7] The low T phase in both cases is now SP. Neutron scattering experiments on $(TMTTF)_2PF_6$ have found that the lattice distortion in the SP state is the expected $2k_F$ BOW distortion, but that the amplitude of the lattice distortion is much smaller[10] than that found in other organic SP materials, such as $MEM(TCNQ)_2$. The exact pattern of the BOW has not been determined yet. Experimental evidence exists that some form of CO persists in the magnetic phases. For example, the splitting in vibronic modes below T_{CO} in $(TMTTF)_2PF_6$ and $(TMTTF)_2AsF_6$, a signature of charge disproportionation, persists into the SP phase,[17] indicating coexistence of CO and SP. At the same time, the high T_{CO} is in competition with the SP ground state,[8] as is inferred from the different effects of pressure on T_{CO} and T_{SP}: while pressure reduces T_{CO}, it *increases* T_{SP}. This is in clear contrast to the effect of pressure on T_N in $X=SbF_6$. Similarly, deuteration of the hydrogen atoms of TMTTF increases T_{CO} but decreases[6,47] T_{SP}. That higher T_{CO} is accompanied by lower T_{SP} for centrosymmetric X ($T_{SP}=16.4$ K in $X=PF_6$ and 11.1 K in $X=AsF_6$) has also been noted.[48] This trend is in obvious agreement with the occurrence of AFM instead of SP state under ambient pressure in $X=SbF_6$. Most interestingly, Nakamura *et al.* have very recently observed redistribution of the charges on the TMTTF molecules in $(TMTTF)_2AsF_6$ and $(TMTTF)_2PF_6$ as these systems enter the SP phase from CO states.[15,16] Charge disproportionation, if any, in the SP phase is much smaller than in the CO phase,[15,16] which is in apparent agreement with the above observations[9,14] in $X=ReO_4$ and SbF_6.

The bulk of the $(TMTTF)_2X$, therefore, lie in the AFM1 and SP regions of Fig. 1. $(TMTSF)_2X$, in contrast, occupy the AFM2 region. Coexisting $2k_F$ CDW and spin-density wave, SDW, with the *same* $2k_F$ periodicity[49,50] here is explained naturally as the $\cdots 1100 \cdots$ BCSDW.[21,22,51] In contrast to the TMTTF salts discussed above, charge and magnetic orderings, in $(TMTTF)_2Br$ occur almost simultaneously.[46,52] X-ray studies of lattice distortions point to similarities with $(TMTSF)_2PF_6$,[49] indicating that $(TMTTF)_2Br$ is also a $\cdots 1100 \cdots$ BCSDW.[21] We do not discuss the AFM2 region in the present paper, as this can be found in our earlier work.[21,25]

III. THEORETICAL MODEL AND CONJECTURES

The one-dimensional (1D) Hamiltonian we investigate is written as

$$H = H_{SSH} + H_{Hol} + H_{ee}, \tag{1a}$$

$$H_{SSH} = t\sum_i [1 + \alpha(a_i^\dagger + a_i)](c_{i,\sigma}^\dagger c_{i+1,\sigma} + \text{H.c.}), + \hbar\omega_S \sum_i a_i^\dagger a_i, \tag{1b}$$

$$H_{Hol} = g\sum_i (b_i^\dagger + b_i) n_i + \hbar\omega_H \sum_i b_i^\dagger b_i, \tag{1c}$$

$$H_{ee} = U\sum_i n_{i,\uparrow} n_{i,\downarrow} + V\sum_i n_i n_{i+1}. \tag{1d}$$

In the above, $c_{i,\sigma}^\dagger$ creates an electron with spin σ ($\uparrow\downarrow$) on molecular site i, $n_{i,\sigma}=c_{i,\sigma}^\dagger c_{i,\sigma}$ is the number of electrons with spin σ on site i, and $n_i=\Sigma_\sigma n_{i,\sigma}$. U and V are the on-site and intersite Coulomb repulsions, and $a_i^\dagger$ and $b_i^\dagger$ create (dispersionless) Su-Schrieffer-Heeger (SSH)[53] and Holstein (Hol)[54] phonons on the ith bond and site, respectively, with frequencies ω_S and ω_H. Because the Peierls instability involves only phonon modes near $q=\pi$, keeping single dispersionless phonon modes is sufficient for the Peierls transitions to occur.[55,56] Although purely 1D calculations cannot yield a finite temperature phase transition, as in all low dimensional theories,[57,58] we anticipate that the 3D ordering in the real system is principally determined by the dominant 1D instability.

The above Hamiltonian includes the most important terms necessary to describe the family of quasi-1D CTS, but ignores nonessential terms that may be necessary for understanding the detailed behavior of individual systems. Such nonessential terms include (i) the intrinsic dimerization that characterizes many $(TMTTF)_2X$, (ii) interaction between counterions and the carriers on the quasi-1D cations stacks, (iii) interchain Coulomb interaction, and (iv) interchain hopping. Inclusion of the intrinsic dimerization will make the Wigner crystal ground state even less likely,[24] and this is the reason for excluding it. We have verified the conclusions of Ref. 24 from exact diagonalization calculations. The inclusion of interactions with counterions may enhance the Wigner crystal ordering[5,23] for some $(TMTTF)_2X$. We will discuss this point further below, and argue that it is important in the AFM1 region of the phase diagram. The effects of intrinsic dimerization and counterion interactions can be reproduced by modifying the $V/|t|$ in our Hamiltonian, and thus these are not included explicitly, rather the V in Eq. (1a) should be considered as the effective V for the quasi-1D

CTS. Interchain hopping, at least in the TMTTF (though not in the TMTSF), are indeed negligible. The interchain Coulomb interaction can promote the Wigner crystal within a rectangular lattice framework, but for the realistic nearly triangular lattice will cause frustration, thereby making the BCDW state of interest here even more likely. We, therefore, believe that Hamiltonian (1a) captures the essential physics of the quasi-1D CTS.

For applications to the quasi-1D CTS, we will be interested in the parameter regime[18,24–26] $|t|=0.1-0.25$ eV, $U/|t|=6-8$. The exact value of V is less known, but since the same cationic molecules of interest as well as other related molecules (e.g., HMTTF, HMTSF, etc.) also form quasi-1D $\frac{1}{2}$-filled band Mott-Hubbard semiconductors with short-range antiferromagnetic spin correlations,[59,60] it must be true that $V<\frac{1}{2}U$ (since for $V>\frac{1}{2}U$ the 1D $\frac{1}{2}$-filled band is a CDW[61,62]). Two other known theoretical results now fix the range of V that will be of interest. First, the ground state of the $\frac{1}{4}$-filled band within Hamiltonian (1a) in the limit of zero e-p coupling is the Wigner crystal $\cdots 1010 \cdots$ only for sufficiently large $V>V_c(U)$. Second, $V_c(U\rightarrow\infty)=2|t|$, and is larger for finite U.[19,24,25] With the known $U/|t|$ and the above restrictions in place, it is now easily concluded that (i) the Wigner crystal is obtained in the CTS for a relatively narrow range of realistic parameters, and (ii) even in such cases the material's V is barely larger than $V_c(U)$.[24,25]

We now go beyond the above ground state theories of spatial broken symmetries to make the following crucial observation: each different spin subspace of Hamiltonian (1a) must have its own V_c at which the Wigner crystal is formed. This conclusion of a *spin-dependent* $V_c=V_c(U,S)$ follows from the comparison of the ferromagnetic subspace with total spin $S=S_{max}$ and the $S=0$ subspace. The ferromagnetic subspace is equivalent to the $\frac{1}{2}$-filled spinless fermion band, and therefore $V_c(U,S_{max})$ is independent of U and exactly $2|t|$. The increase of $V_c(U,S=0)$ with decreasing U (Refs. 19 and 25) is then clearly related to the occurrence of doubly occupied and vacant sites at finite U in the $S=0$ subspace. Since the probability of double occupancy (for fixed U and V) decreases monotonically with increasing S, we can interpolate between the two extreme cases of $S=0$ and $S=S_{max}$ to conclude $V_c(U,S)>V_c(U,S+1)$. We prove this explicitly from numerical calculations in the next section.

Our conjecture regarding spin-dependent $V_c(U)$ in turn implies that there exist three distinct parameter regimes for realistic U and V: (i) $V\leqslant V(S_{max})=2|t|$, in which case the ground state is the BCDW with $2k_F$ CO and the high-temperature $4k_F$ state is a BOW;[18,25] (ii) $V>V_c(U,S=0)$, in which case both the $4k_F$ and the $2k_F$ phases have Wigner crystal CO; (iii) and the intermediate regime $2|t|\leqslant V\leqslant V_c(U,S=0)$. Parameter regime (i) has been discussed in our previous work.[18,21,25,63] This is the case where the description of the $\frac{1}{4}$-filled band as an effective $\frac{1}{2}$-filled band is appropriate: the unit cell in the $4k_F$ state is a dimer of two sites, and the $2k_F$ transition can be described as the usual SP dimerization of the dimer lattice. We will not discuss this parameter region further. Given the $U/|t|$ values for the CTS, parameter regime (ii) can have rather narrow width. For $U/|t|=6$, $V_c(U,S=0)=3.3|t|$, and there is no value of realistic V for which the ground state is a Wigner crystal. For $U/|t|=8$, $V_c(U,S=0)=3.0|t|$, and the widths of parameter regime (iii), $2|t|\leqslant V\leqslant 3|t|$, and of parameter regime (ii), $3|t|\leqslant V\leqslant 4|t|$, are comparable.

We will discuss parameter regime (ii) only briefly, as the physics of this region has been discussed by other authors.[20,26] We investigated thoroughly the intermediate parameter regime (iii), which has not been studied previously. Within the intermediate parameter regime, we expect a transition from the BCDW in the $2k_F$ state at low T to a $\cdots 1010 \cdots$ CO in the $4k_F$ phase at high T that has not been discussed in the theoretical literature.

Our observation regarding the T-dependent behavior of these CTS follows from the more general observation that thermodynamic behavior depends on the free energy and the partition function. For the strong e-e interactions of interest here, thermodynamics of 1D systems at temperatures of interest is determined almost entirely by spin excitations. Since multiplicities of spin states increase with the total spin S, the partition function is dominated by high (low) spin states with large (small) multiplicities at high (low) temperatures. While at $T=0$ such a system must be a BCDW for $V<V_c(U,S=0)$, as the temperature is raised, higher and higher spin states begin to dominate the free energy, until V for the material in question exceeds $V_c(U,S)$, at which point the charge occupancy reverts to $\cdots 1010 \cdots$ We demonstrate this explicitly in the next section. A charge redistribution is *expected* in such a system at T_{2k_F}, as the deviation from the average charge of 0.5 is much smaller in the BCDW than in the Wigner crystal.[25]

The above conjecture leads to yet another implication. The ground state for both weak and intermediate intersite Coulomb interaction parameters are the BCDW, even as the $4k_F$ phases are different in the two cases: BOW in the former and CO in the latter. This necessarily requires the existence of two different kinds of spin excitations from the BCDW. Recall that within the standard theory of the SP transition in the $\frac{1}{2}$-filled band,[57,64,65] thermal excitations from the $T=0$ ground state generates spin excitations with bond-alternation domain walls (solitons), with the phase of bond alternation in between the solitons being opposite to that outside the solitons. Progressive increase in T generates more and more solitons with reversed bond alternation phases, until overlaps between the two phases of bond-alternations lead ultimately to the uniform state. A key difference between the $\frac{1}{2}$-filled and $\frac{1}{4}$-filled SP states is that site charge occupancies in spin excitations in the former continue to be uniform, while they are necessarily nonuniform in the latter case, as we show in the next section. We demonstrate that defect centers with two distinct charge occupancies (that we will term as types I and II), depending upon the actual value of V, are possible in the $\frac{1}{4}$-filled band. Preponderance of one or another type of defects generates the distinct $4k_F$ states.

IV. RESULTS

We present in this section the results of QMC investigations of Eq. (1), for both zero and nonzero e-p couplings, and

of ED studies of the adiabatic (semiclassical) limit of Eq. (1a). Using QMC techniques, we demonstrate explicitly the spin dependence of $V_c(U)$, as well as the transition from the Wigner crystal to the BCDW for the intermediate parameter regime (iii). The ED studies demonstrate the exotic nature of spin excitations from the BCDW ground state. In what follows, all quantities are expressed in units of $|t|$ ($|t|=1$).

The QMC method we use is the stochastic series expansion (SSE) method using the directed-loop update for the electron degrees of freedom.[66] For 1D fermions with nearest-neighbor hopping SSE provides statistically exact results with no systematic errors. While the SSE directed-loop method is grand canonical (with fluctuating particle density), we restrict measurements to only the $\frac{1}{4}$-filled density sector to obtain results in the canonical ensemble. Quantum phonons are treated within SSE by directly adding the bosonic phonon creation and annihilation operators in Eq. (1a) to the series expansion.[67] An upper limit in the phonon spectrum must be imposed, but can be set arbitrarily large to avoid any systematic errors.[67] For the results shown below, we used a cutoff of 100 SSH phonons per bond and either 30 (for $g=0.5$) or 50 (for $g=0.75$) Holstein phonons per site.

The observables we calculate within SSE are the standard wave-vector-dependent charge structure factor $S_\rho(q)$, defined as

$$S_\rho(q) = \frac{1}{N}\sum_{j,k} e^{iq(j-k)}\langle O_j^\rho O_k^\rho\rangle, \tag{2}$$

and charge and bond-order susceptibilities $\chi_\rho(q)$ and $\chi_B(q)$, defined as

$$\chi_x(q) = \frac{1}{N}\sum_{j,k} e^{iq(j-k)}\int_0^\beta d\tau\langle O_j^x(\tau)O_k^x(0)\rangle. \tag{3}$$

In Eqs. (2) and (3), N is the number of lattice sites, $O_j^\rho = n_{j,\uparrow}+n_{j,\downarrow}$, $O_j^B = \Sigma_\sigma(c_{j+1,\sigma}^\dagger c_{j,\sigma}+\text{H.c.})$, and β is the inverse temperature in units of t.

The presence of CO or BOW can be detected by the divergence of the $2k_F$ or $4k_F$ charge or bond-order susceptibility as a function of increasing system size. Strictly speaking, in a purely 1D model, these functions diverge only at $T=0$; as already explained above, we make the reasonable assumption[58] that in the presence of realistic interchain couplings transitions involving charge or bond-order instabilities, as determined by the dominant susceptibility, occur at finite T.

A. Spin-dependent $V_c(U)$

We first present computational results within Hamiltonian (1a) in the absence of e-p coupling to demonstrate that the $V_c(U)$ at which the Wigner crystal order is established in the lowest state of a given spin subspace decreases with increasing spin S. Our computational approach conserves the total z component of spin S_z and not the total S. Since the Lieb-Mattis theorem[68] $E(S)<E(S+1)$, where $E(S)$ is the energy of the lowest state in the spin subspace S, applies to the 1D Hamiltonian (1a), and since in the absence of a magnetic field all S_z states for a given S are degenerate, our results for the lowest state within each different S_z must pertain to $S=S_z$.

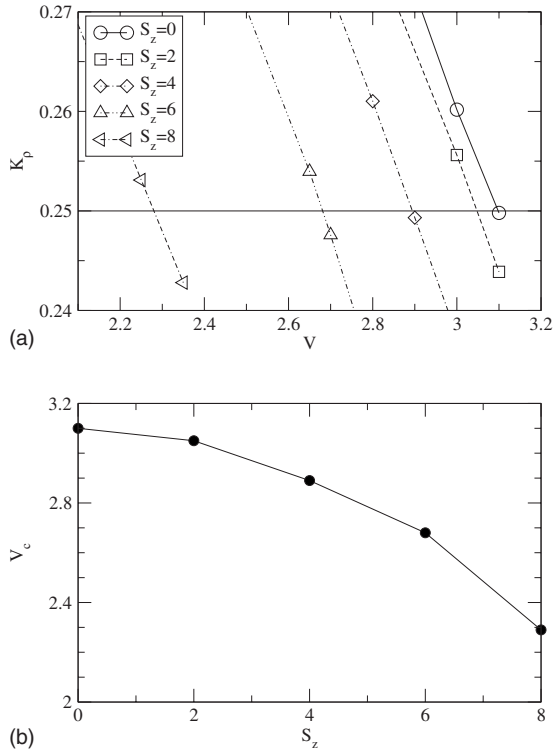

FIG. 2. V_c for Eq. (1a) in the limit of zero e-p interactions ($\alpha=g=0$) as a function of S_z. Results are for a $N=32$ site periodic ring with $U=8$. For $N=32$ $S_z=8$ corresponds to the fully polarized (spinless fermion) limit. (a) Luttinger Liquid exponent K_ρ as a function of V. $K_\rho=\frac{1}{4}$ determines the boundary for the $\cdots 1010\cdots$ CO phase. (b) V_c plotted vs. S_z.

To determine $V_c(U,S)$, we use the fact that the purely electronic model is a Luttinger liquid (LL) for $V<V_c$ with correlation functions determined by a single exponent K_ρ (see Ref. 69 for a review). The Wigner crystal state is reached when $K_\rho=\frac{1}{4}$. The exponent K_ρ may be calculated from the long-wavelength limit of $S_\rho(q)$.[70] In Fig. 2(a), we have plotted our calculated K_ρ for $U=8$ as a function of V for different S_z sectors. The temperature chosen is small enough ($\beta=2N$) that in all cases the results correspond to the lowest state within a given S_z. In Fig. 2(b), we have plotted our calculated $V_c(U=8)$, as obtained from Fig. 2(a), as a function of S_z. V_c is largest for $S_z=0$ and decreases with increasing S_z, in agreement with the conjecture of Sec. III. Importantly, the calculated V_c for $S_z=8$ is close to the correct limiting value of 2, indicating the validity of our approach. We have not performed any finite-size scaling in Fig. 2, which accounts for the the slight deviation from the exact value of 2.

B. T-dependent susceptibilities

We next present the results of QMC calculations within the full Hamiltonian (1a). To reproduce correct relative energy scales of intra- and intermolecular phonon modes in the CTS, we choose $\omega_H > \omega_S$, specifically $\omega_H=0.5$ and $\omega_S=0.1$

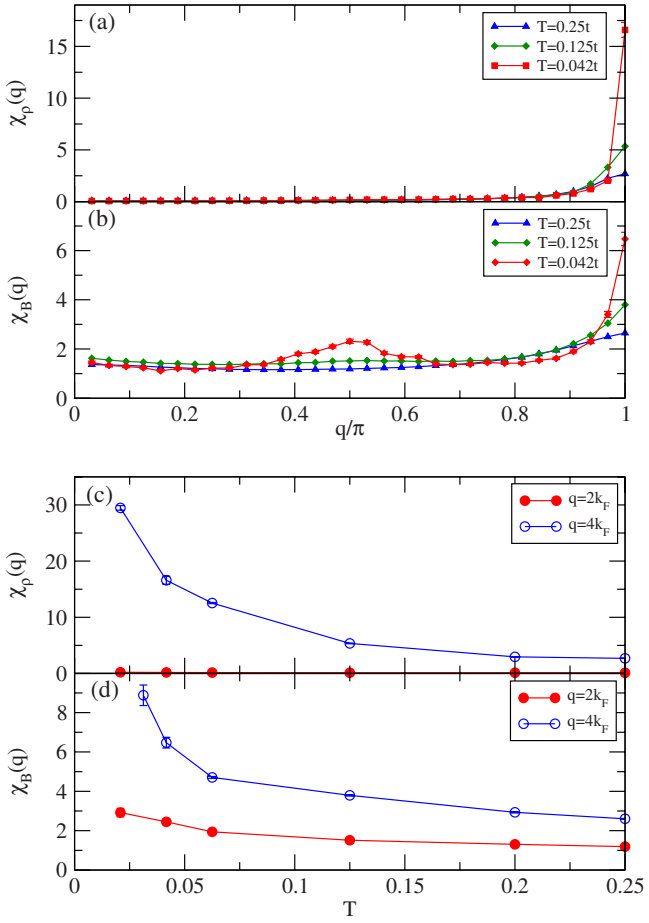

FIG. 3. (Color online) QMC results for the temperature-dependent charge susceptibilities for a $N=64$ site periodic ring with $U=8$, $V=2.75$, $\alpha=0.15$, $\omega_S=0.1$, $g=0.5$, and $\omega_H=0.5$. (a) and (b) Wave-vector-dependent charge and bond-order susceptibilities. (c) $2k_F$ and $4k_F$ charge susceptibilities as a function of temperature. (d) $2k_F$ and $4k_F$ bond-order susceptibilities as a function of temperature. If error bars are not shown, statistical error bars are smaller than the symbol sizes. Lines are guides to the eye.

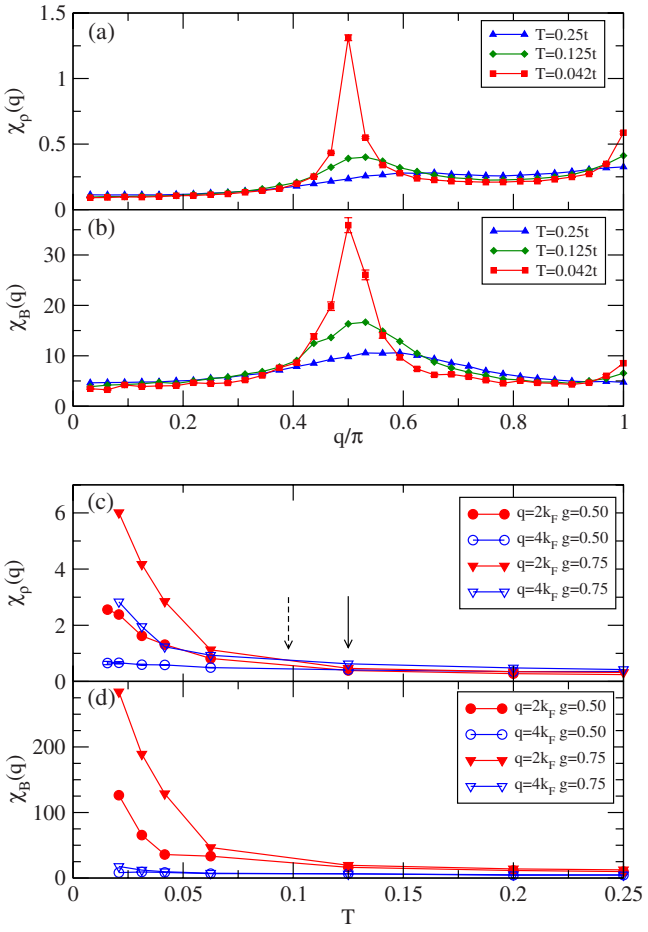

FIG. 4. (Color online) Same as Fig. 3, but with parameters $U=8$, $V=2.25$, $\alpha=0.27$, $\omega_S=0.1$, and $\omega_H=0.5$. In panels (a) and (b), data are for $g=0.50$ only. In panels (c) and (d), data for both $g=0.50$ and $g=0.75$ are shown. Arrows indicate temperature where $\chi_\rho(2k_F)=\chi_\rho(4k_F)$ (solid and broken arrows correspond to $g=0.50$ and 0.75, respectively.)

in our calculations. Small deviations from these values do not make any significant difference. In all cases, we have chosen the electron-molecular vibration coupling g larger than the coupling between electrons and the SSH phonons α, thereby deliberately enhancing the likelihood of the Wigner crystal CO. We report results only for intermediate and strong weak intersite Coulomb interactions; the weak interaction regime $V<2$ has been discussed extensively in our previous work.[25]

1. $2 \leqslant V \leqslant V_c(U,S=0)$

Our results are summarized in Figs. 3–5, where we report results for two different V of intermediate strength and several different e-p couplings. Figure 3 first shows results for relatively weak SSH coupling α. The charge susceptibility is dominated by a peak at $4k_F=\pi$ [Fig. 3(a)]. Figures 3(c) and 3(d) show the T dependence of the $2k_F$ as well as $4k_F$ charge and bond susceptibilities. For $V<V_c(U,S=0)$, the $4k_F$ charge susceptibility does not diverge with system size, and the purely 1D system remains a LL with no long-range CO at zero temperature. The dominance of $\chi_\rho(4k_F)$ over $\chi_\rho(2k_F)$ suggests, however, that $\cdots 1010 \cdots$ CO will likely occur in the 3D system, especially if this order is further enhanced due to interactions with the counterions.[9] We have plotted the bond susceptibilities $\chi_B(2k_F)$ and $\chi_B(4k_F)$ in Fig. 3(d). A SP transition requires that $\chi_B(2k_F)$ diverges as $T \to 0$. $\chi_B(2k_F)$ weaker than $\chi_B(4k_F)$ at low T indicates that the SP order is absent in the present case with weak SSH e-p coupling. This result is in agreement with an earlier result[55] that the SP order is obtained only above a critical α_c (α_c may be smaller for the infinite system than found in our calculation). The most likely scenario with the present parameters is the persistence of the $\cdots 1010 \cdots$ CO to the lowest T with no SP transition. These parameters, along with counterion interactions, could then describe the $(TMTTF)_2X$ materials with an AFM ground state.[9]

In Figs. 4 and Fig. 5, we show our results for larger SSH e-p coupling α and two different intersite Coulomb interactions $V=2.25$ and 2.75. The calculations of Fig. 4 were done for two different Holstein e-p couplings g. For both the V

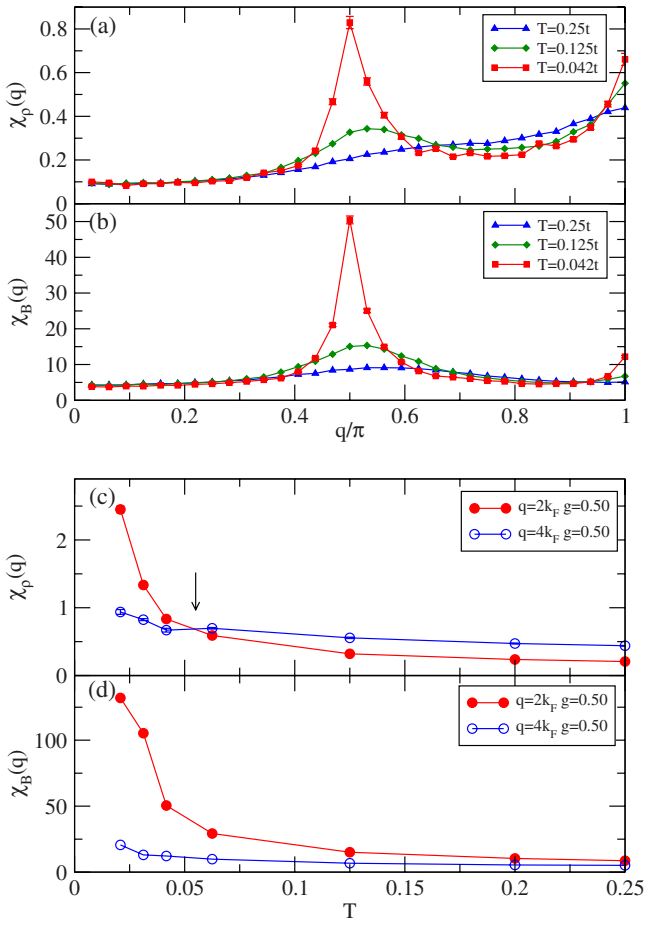

FIG. 5. (Color online) Same as Fig. 3, but with parameters $U=8$, $V=2.75$, $\alpha=0.27$, $\omega_S=0.1$, $g=0.5$, and $\omega_H=0.5$. Arrow indicates temperature where $\chi_\rho(2k_F)=\chi_\rho(4k_F)$.

parameters, $\chi_\rho(4k_F)$ dominates at high T but $\chi_\rho(2k_F)$ is stronger at low T in both Figs. 4(c) and 5(c). The crossing between the two susceptibilities is a clear indication that in the intermediate parameter regime, as T is lowered the $2k_F$ CDW instability dominates over the $4k_F$ CO.

The rise in $\chi_\rho(2k_F)$ at low T is accompanied by a steep rise in $\chi_B(2k_F)$ in both cases [see Figs. 4(d) and 5(d)]. Importantly, unlike in Fig. 3(d), $\chi_B(2k_F)$ in these cases clearly dominates over $\chi_B(4k_F)$ by an order of magnitude at low temperatures. There is thus a clear signature of the SP instability for these parameters. The *simultaneous* rise in $\chi_B(2k_F)$ and $\chi_\rho(2k_F)$ indicates that the SP state is the $\cdots 1100 \cdots$ BCDW. Comparison of Figs. 4 and 5 indicates that the effect of larger V is to decrease the T, where the $2k_F$ and $4k_F$ susceptibilities cross. Since larger V would imply larger T_{CO}, this result implies that larger T_{CO} is accompanied by lower T_{SP}. Our calculations are for relatively modest $\alpha < g$. Larger α (not shown) further strengthens the divergence of $2k_F$ susceptibilities.

The motivation for performing the calculations of Fig. 4 with multiple Holstein couplings was to determine whether it is possible to have a Wigner crystal at low T even for $V < V(U,S=0)$, by simply increasing g. The argument for this would be that in strong coupling, increasing g amounts to an effective increase in V.[71] The Holstein coupling cannot be increased arbitrarily; however, as beyond a certain point, g promotes formation of on-site bipolarons.[67] Importantly, the cooperative interaction between the $2k_F$ BOW and CDW in the BCDW[21,25] implies that in the $V < V(U,S=0)$ region, larger g not only promotes the $4k_F$ CO but also enhances the BCDW. In our calculations in Figs. 4(b) and 4(c), we find both these effects: a weak increase in $\chi_\rho(4k_F)$ at intermediate T and an even stronger increase in the $T \to 0$ values of $\chi_\rho(2k_F)$ and $\chi_B(2k_F)$. Actually, this result is in qualitative agreement with our observation for the ground state within the adiabatic limit of Eq. (1a) that in the range $0 < V < V(U,S=0)$, V enhances the BCDW.[25] The temperature at which $\chi_\rho(2k_F)$ and $\chi_\rho(4k_F)$ cross does not change significantly with larger g. Our results for $g=0.75$ for $V=2.75$ (not shown) are similar, except that the data are more noisy now (probably because all parameters in Fig. 5 are much too large for the larger g). We conclude, therefore, that in the intermediate V region, merely increasing g does not change the BCDW nature of the SP state. For g to have a qualitatively different effect, V should be much closer to $V(U,S=0)$ or perhaps even larger.

2. $V > V_c(U,S=0)$

In principle, calculations of low-temperature instabilities here should be as straightforward as the weak intersite Coulomb interaction $V < 2t$ regime. The $4k_F$ CO-AFM1 state $\uparrow 0 \downarrow 0$ would occur naturally for the case of weak e-p coupling. Obtaining the $4k_F$ CO-SP state $1=0=1 \cdots 0 \cdots 1$, with *realistic* $V < \frac{1}{2}U$ is, however, difficult.[25] Previous work,[72] for example, finds this state for $V > \frac{1}{2}U$. Recent T-dependent mean-field calculations of Seo *et al.*[39] also fail to find this state for nonzero V. There are two reasons for this. First, the spin exchange here involves charge-rich sites that are *second neighbors* and are hence necessarily small. Energy gained upon alternation of this weak exchange interactions is even smaller, and thus the tendency to this particular form of the SP transition is weak to begin with. Second, this region of the parameter space involves either large U [e.g., $U=10$, for which $V_c(U,S=0) \simeq 2$] or relatively large V [e.g., $V_c(U,S=0) \simeq 3$ for $U=8$]. In either case, such strong Coulomb interactions make the applicability of mean-field theories questionable.

Our QMC calculations do find the tendency to SP instability in this parameter region. In Fig. 6, we show QMC results for $V > V_c(U=8,S=0)$. In contrast to Figs. 4 and 5, $\chi_\rho(4k_F)$ now dominates over $\chi_\rho(2k_F)$ at all T. The weaker peak at $q=2k_F$ at low T is due to small differences in site charge populations between the charge-poor sites of the Wigner crystal that arises upon bond distortion,[25] and that adds a small period four component to the charge modulation. The bond susceptibility $\chi_B(q)$ has a strong peak at $2k_F$ and a weaker peak at $4k_F$, exactly as expected for the $4k_F$ CO-SP state. Previous work has shown that the difference in charge densities between the charge-rich and charge-poor sites in the $4k_F$ CO-SP ground state is considerably larger than in the BCDW.[25]

C. Spin excitations from the bond-charge-density wave

The above susceptibility calculations indicate that in the intermediate V region (Figs. 4 and 5) the BCDW ground

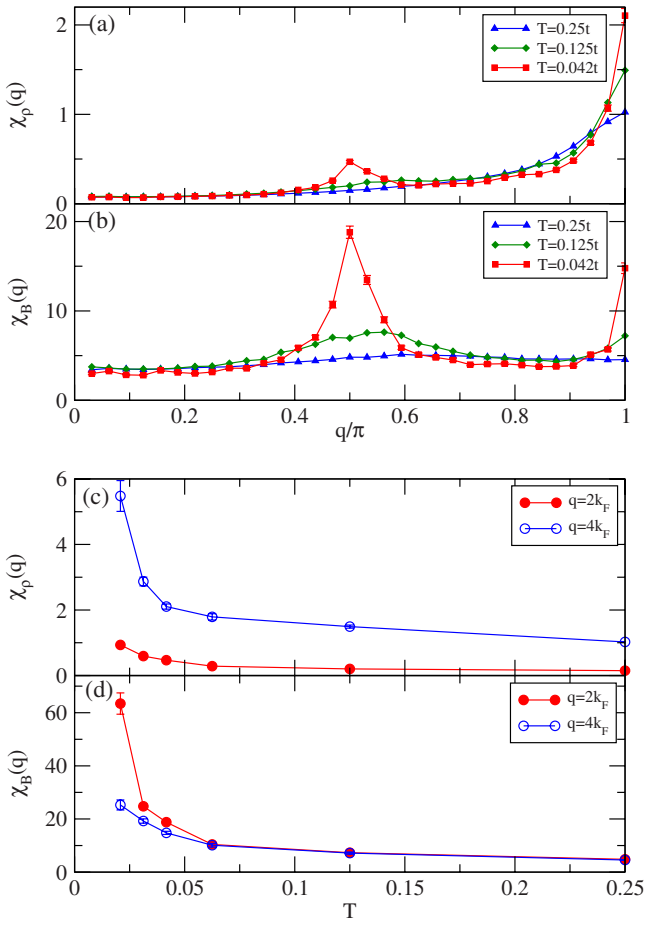

FIG. 6. (Color online) Same as Fig. 3, but with parameters $U=8$, $V=3.5$, $\alpha=0.24$, $\omega_S=0.1$, $g=0.5$, and $\omega_H=0.5$.

state with $\cdots 1100 \cdots$ CO can evolve into the $\cdots 1010 \cdots$ CO as T increases. Our earlier work had shown that for weak V, the BCDW evolves into the $4k_F$ BOW at high T.[18,25] Within the standard theory of the SP transition,[57,64,65] applicable to the $\frac{1}{2}$-filled band, the SP state evolves into the undistorted state for $T > T_{SP}$. Thus, the $4k_F$ distortions, CO and BOW, take the role of the undistorted state in the $\frac{1}{4}$-filled band, and it appears paradoxical that the same ground state can evolve into two different high T states. We show here that this is intimately related to the nature of the spin excitations in the $\frac{1}{4}$-filled BCDW. Spin excitations from the conventional SP state leave the site charge occupancies unchanged. We show below that not only do spin excitations from the $\frac{1}{4}$-filled BCDW ground state lead to changes in the site occupancies, but also two different kinds of site occupancies are possible in the localized defect states that characterize spin excited states here. We will refer to these as type I and type II defects, and depending on which kind of defect dominates at high T (which in turn depends on the relative magnitudes of V and the e-p couplings), the $4k_F$ state is either the CO or the BOW.

We will demonstrate the occurrence of type I and II defects in spin excitations numerically. Below, we present a physical intuitive explanation of this highly unusual behavior, based on a configuration space picture. Very similar configuration space arguments can be found elsewhere in our discussion of charge excitations from the BCDW in the interacting $\frac{1}{4}$-filled band.[73]

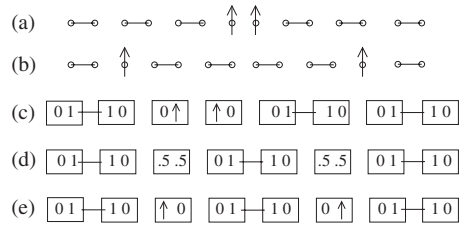

FIG. 7. [(a) and (b)] $S=1$ VB diagram in the Heisenberg SP chain. The SP bond order in between the $S=\frac{1}{2}$ solitons in (b) is opposite to that elsewhere. (c) $\frac{1}{4}$-filled band equivalent of (a); the singlet bonds in the background BCDW are between units containing a pair of sites but a single electron (see text). [(d) and (e)] $\frac{1}{4}$-filled band equivalents of (b). Defect units with two different charge distributions are possible. The charge distribution will depend on V.

We begin our discussion with the standard $\frac{1}{2}$-filled band, for which the mechanism of the SP transition is well understood.[57,64,65] Figure 7(a) shows in valence bond (VB) representation the generation of a spin triplet from the standard $\frac{1}{2}$-filled band. Since the two phases of bond alternation are isoenergetic, the two free spins can separate, and the true wave function is dominated by VB diagrams as in Fig. 7(b), where the phase of the bond alternation in between the two unpaired spins (spin solitons) is opposite to that in the ground state. With increasing temperature and increasing number of spin excitations, there occur many such regions with reversed bond alternations, and overlaps between regions with different phases of bond alternations lead ultimately to the uniform state.

The above picture needs to be modified for the dimerized dimer BCDW state in the $\frac{1}{4}$-filled band, in which the single site of the $\frac{1}{2}$-filled band system is replaced by a dimer unit with site populations 1 and 0 (or 0 and 1), and the stronger interdimer 1-1 bond (weaker interdimer $0 \cdots 0$ bond) corresponds to the strong (weak) bond in the standard SP case. Figure 7(c), showing triplet generation from the BCDW, is the $\frac{1}{4}$-filled analog of Fig. 7(a): a singlet bond between the dimer units has been broken to generate a localized triplet. The effective repulsion between the free spins of Fig. 7(a) is due to the absence of binding between them, and the same is expected in Fig. 7(c). Because the site occupancies *within* the dimer units are nonuniform now, the repulsion between the spins is reduced from changes in *intradimer* as well as interdimer site occupancies: the site populations within the neighboring units can become uniform (0.5 each), or the site occupancies can revert to 1001 from 0110. There is no equivalent of this step in the standard SP case. The next steps in the separation of the resultant defects are identical to that in Fig. 7(b), and we have shown these possible final states in Figs. 7(d) and 7(e), for the two different intraunit spin defect populations. For $V < V_c(U,S)$, defect units with site occupancies 0.5 occupancies (type I defects) are expected to dominate, while for $V > V_c(U,S)$, site populations of 10 and 01 (type II defects) dominate. From the qualitative discussions,

it is difficult to predict whether the defects are free, in which case they are solitons, or if they are bound, in which case two of them constitute a triplet. What is more relevant is that type I defects generate bond dimerization locally (recall that the $4k_F$ BOW has uniform site charge densities), while type II defects generate local site populations 1010, which will have the tendency to generate the $4k_F$ CO.

The process by which the BCDW is reached from the $4k_F$ BOW or the CO as T is decreased from T_{2k_F} is exactly opposite to the discussion of spin excitations from the BCDW in Fig. 7. Now $\cdots 1100 \cdots$ domain walls appear in the background bond-dimerized or charge-dimerized state. In the case of the $\cdots 1010 \cdots$ $4k_F$ state, the driving force for the creation of such a domain wall is the energy gained upon singlet formation [for $V < V_c(U,S)$].

Figure 7(e) suggests the appearance of localized $\cdots 1010 \cdots$ regions in excitations from the $\cdots 1100 \cdots$ BCDW SP state for $2|t| \leqslant V \leqslant V_c(U, S=0)$. We have verified this with exact spin-dependent calculations for $N=16$ and 20 periodic rings with adiabatic e-p couplings,

$$H^A_{SSH} = t\sum_i [1 - \alpha(u_i - u_{i+1})](c^\dagger_{i,\sigma} c_{i+1,\sigma} + \text{H.c.}) + \frac{1}{2} K_S \sum_i (u_i - u_{i+1})^2, \tag{4a}$$

$$H^A_{Hol} = g\sum_i v_i n_i + \frac{1}{2} K_H \sum_i v_i^2, \tag{4b}$$

and H_{ee} as in Eq. (1d). In the above, u_i is the displacement from equilibrium of a molecular unit and v_i is a molecular mode. Note that due to the small sizes of the systems, we are able to solve exactly the e-p couplings in Eq. (4a) and Eq. (4b) cannot be directly compared to those in Eq. (1a). In the present case, we take the smallest e-p couplings necessary to generate the BCDW ground state self-consistently within the adiabatic Hamiltonian.[22,23,25] We then determine the bond distortions, site charge occupancies, and spin-spin correlations self-consistently with the same parameters for excited states with $S_z > 0$.

In Fig. 8(a), we have plotted the deviations of the site charge populations from average density of 0.5 for the lowest $S_z=2$ state for $N=20$, for $U=8$, $V=2.75$, and e-p couplings as given in the figure caption. Deviations of the charge occupancies from the perfect $\cdots 0110 \cdots$ sequence identify the defect centers, as seen from Figs. 7(c)–7(e). In the following, we refer to dimer units composed of sites i and j as $[i,j]$. Based on the charge occupancies in the figure, we identify units [1,2], [7,8], [13,14], and [14,15] as the defect centers. Furthermore, based on site populations of nearly exactly 0.5, we identify defects on units [1,2] and [7,8] as type I; the populations on units [13,14] and [14,15] identify them as type II. Type I defects appear to be free and solitonlike, while type II defects appear to be bound into a triplet state, but both could be finite-size effects.

Figures 7(d) and 7(e) suggest that the spin-spin z-component correlations, $\langle S^z_i S^z_j \rangle$, are large and positive only between pairs of sites which belong to the defect centers, as

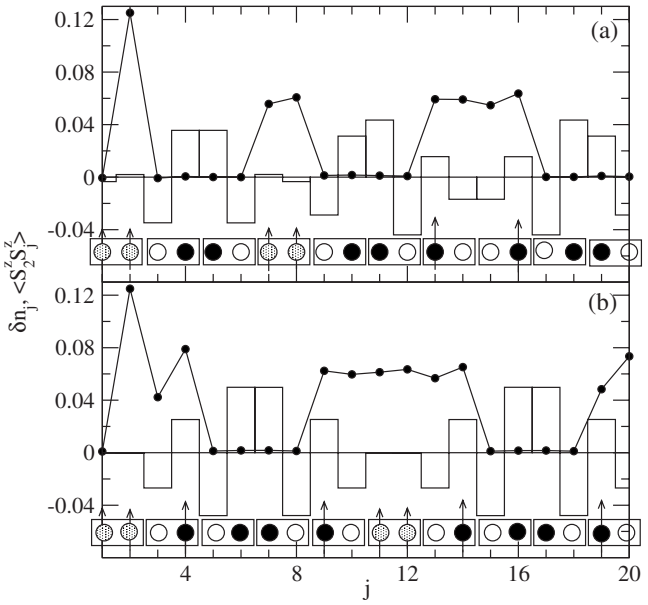

FIG. 8. (a) Self-consistent site charges (vertical bars) and spin-spin correlations (points, lines are to guide the eye) in the $N=20$ periodic ring with $U=8$, $V=2.75$, $\alpha^2/K_S=1.5$, $g^2/K_H=0.32$ for $S_z=2$. (b) Same parameters, except $S_z=3$. Black and white circles at the bottoms of the panels denote charge-rich and charge-poor sites, respectively, while gray circles denote sites with population nearly exactly 0.5. The arrows indicate locations of the defect units with nonzero spin densities.

all other spins are singlet coupled. For our characterization of units [1,2], [7,8], [13,14], and [14,15] to be correct, therefore, $\langle S^z_i S^z_j \rangle$ must be large and positive if sites i and j both belong to this set of sites, and small (close to zero) when either i or j does not belong to this set (as all sites that do not belong to the set are singlet bonded). We have superimposed the calculated z-component spin-spin correlations between site 2 and all sites $j=1-20$. The spin-spin correlations are in complete agreement with our characterization of units [1,2], [7,8], [13,14], and [14,15] as defect centers with free spins. The singlet 1-1 bonds between nearest-neighbor charge-rich sites in Figs. 7(c)–7(e) require that spin-spin couplings between such pairs of sites are large and negative, while spin-spin correlations between one member of the pair any other site is small. We have verified such strong spin-singlet bonds between sites 4 and 5, 10 and 11, and 18 and 19, respectively (not shown). Thus, multiple considerations lead to the identification of the same sites as defect centers, and to their characterization as types I and II.

We report similar calculations in Fig. 8(b) for $S_z=3$. Based on charge occupancies, four out of the six defect units with unpaired spins in the $S_z=3$ state are type II; these occupy units [3,4], [9,10], [13,14], and [19,20]. Type I defects occur on units [1,2] and [11,12]. As indicated in the figure, spin-spin correlations are again large between site 2 and all other sites that belong to this set, while they are again close to zero when the second site is not a defect site. As in the previous case, we have verified singlet spin couplings between nearest-neighbor pairs of charge-rich sites. There occur then exact correspondences between charge densities and spin-spin correlations, exactly as for $S_z=2$.

The susceptibility calculations in Figs. 4 and 5 are consistent with the microscopic calculations of spin defects presented above. As $4k_F$ defects are added to the $2k_F$ background, the $2k_F$ susceptibility peak is expected to broaden and shift toward higher q. This is exactly what is seen in the charge susceptibility, Figs. 4(a) and 5(a), as T is increased. A similar broadening and shift are seen in the bond order susceptibility as well.

V. DISCUSSIONS AND CONCLUSIONS

In summary, the SP state in the $\frac{1}{4}$-filled band CTS is unique for a wide range of realistic Coulomb interactions. Even when the $4k_F$ state is the Wigner crystal, the SP state can be the $\cdots 1100 \cdots$ BOW. For $U=8$, for example, the transition found here will occur for $2<V<3$. This T-dependent transition from the Wigner crystal to the BCDW is a consequence of the spin dependence of V_c. Only for $V>3$ here can the SP phase be the tetramerized Wigner crystal $1=0=1\cdots 0\cdots 1$ (note, however, that $V \leqslant 4$ for $U=8$). We have ignored the intrinsic dimerization along the 1D stacks in our reported results, but this increases $V_c(U,S=0)$ even further, and makes the Wigner crystal that much more unlikely.[24] Although even larger U ($U=10$, for example) reduces $V_c(U,S=0)$, we believe that the Coulomb interactions in the $(TMTTF)_2X$ lie in the intermediate range.

A Wigner crystal to BCDW transition would explain most of the experimental surprises discussed in Sec. II. The discovery of the charge redistribution upon entering the SP phase[15,16] in $X=AsF_6$ and PF_6 is probably the most dramatic illustration of this. Had the SP state maintained the same charge modulation pattern as the Wigner crystal that exist above T_{2k_F}, the difference in charge densities between the charge-rich and the charge-poor sites would have changed very slightly.[25] The dominant effect of the SP transition leading to $1=0=1\cdots 0\cdots 1$ is only on the charge-poor sites, which are now inequivalent (note that the charge-rich sites remain equivalent). The difference in charge density of the charge-rich sites and the average of the charge density of the charge-poor sites thus remains the same.[25] In contrast, the difference in charge densities between the charge-rich and the charge-poor sites in the BCDW is considerably smaller than in the Wigner crystal,[25] and we believe that the experimentally observed smaller charge density difference in the SP phase simply reflects its BCDW character.

The experiments of Refs. 15 and 16 should not be taken in isolation: we ascribe the competition between the CO and the SP states in $X=PF_6$ and AsF_6, as reflected in the different pressure dependences of these states,[8] to their having different site charge occupancies. The observation that the charge density difference in $X=SbF_6$ decreases considerably upon entering the SP phase from the AFM1 phase[9] can also be understood if the AFM1 and the SP phases are assigned to be Wigner crystal and the BCDW, respectively. The correlation between larger T_{CO} and smaller T_{SP} (Ref. 48) is expected. Larger T_{CO} implies larger effective V, which would lower T_{SP}. This is confirmed from comparing Figs. 4 and 5: the temperature at which $\chi_{\rho(2k_F)}$ begins to dominate over $\chi_{\rho(4k_F)}$ is considerably larger in Fig. 4 (smaller V) than in Fig. 5 (larger V). The isotope effect, strong enhancement of the T_{CO} (from 69 to 90 K) with deuteration of the methyl groups in $X=PF_6$, and concomitant decrease in T_{SP} (Refs. 6 and 47) are explained along the same line. Deuteration decreases ω_H in Eq. (1a), which has the same effect as increasing V. Thus, from several different considerations, we come to the conclusion that the transition from the Wigner crystal to the BCDW that we have found here theoretically for intermediate $V/|t|$ does actually occur in $(TMTTF)_2X$ that undergo SP transition. This should not be surprising. Given that the 1:2 anionic CTS lie in the "weak" $V/|t|$ regime, TMTTF with only slightly smaller $|t|$ (but presumably very similar V, since intrastack intermolecular distances are comparable in the two families) lies in the "intermediate" as opposed to "strong" $V/|t|$ regime.

Within our theory, the two different antiferromagnetic regions that straddle the SP phase in Fig. 1, AFM1 and AFM2, have different charge occupancies. The Wigner crystal character of the AFM1 region is revealed from the similar behavior of T_N and T_{CO} in $(TMTTF)_2SbF_6$ under pressure,[9] indicating the absence of the competition of the type that exists between CO and SP, in agreement with our assignment. The occurrence of a Wigner crystal AFM1 instead of SP does not necessarily imply a larger $V/|t|$ in the SbF_6. A more likely reason is that the interaction with the counterions is strong here, and this interaction together with V pins the electrons on alternate sites. $(TMTSF)_2X$, and possibly $(TMTTF)_2Br$, belong to the AFM2 region. The observation that the CDW and the spin-density wave in the TMTSF have the same periodicities[1] had led to the conclusion that the charge occupancy here is $\cdots 1100 \cdots$.[21] This conclusion remains unchanged. Finally, we comment that the observation of Wigner crystal CO[3] in $(DI\text{-}DCNQI)_2Ag$ is not against our theory, as the low T phase here is antiferromagnetic and not SP. We predict the SP system $(DMe\text{-}DCNQI)_2Ag$ to have the $\cdots 1100 \cdots$ charge ordering.

In summary, it appears that the key concept of spin-dependent V_c within Eq. (1a) can resolve most of the mysteries associated with the temperature dependence of the broken symmetries in the $\frac{1}{4}$-filled band CTS. One interesting feature of our work involves demonstration of spin excitations from the BCDW state that necessarily lead to local changes in site charges. Even for weak Coulomb interactions, the $\frac{1}{4}$-filled band has the BCDW character.[18] The effects of magnetic field on $\frac{1}{4}$-filled band CDWs is of strong recent interest.[74,75] We are currently investigating the consequences of the Zeeman interaction on the mixed spin-charge excitations of the BCDW.

ACKNOWLEDGMENTS

We acknowledge illuminating discussions with S. E. Brown. This work was supported by the Department of Energy Grant No. DE-FG02-06ER46315 and the American Chemical Society Petroleum Research Fund.

[1] J. P. Pouget and S. Ravy, J. Phys. I **6**, 1501 (1996).
[2] B. Dumoulin, C. Bourbonnais, S. Ravy, J. P. Pouget, and C. Coulon, Phys. Rev. Lett. **76**, 1360 (1996).
[3] K. Hiraki and K. Kanoda, Phys. Rev. Lett. **80**, 4737 (1998); T. Kakiuchi, Y. Wakabayashi, H. Sawa, T. Itou, and K. Kanoda, *ibid.* **98**, 066402 (2007).
[4] F. Nad and P. Monceau, J. Phys. Soc. Jpn. **75**, 051005 (2006), and references therein.
[5] P. Monceau, F. Y. Nad, and S. Brazovskii, Phys. Rev. Lett. **86**, 4080 (2001).
[6] F. Nad, P. Monceau, T. Nakamura, and K. Furukawa, J. Phys.: Condens. Matter **17**, L399 (2005).
[7] D. S. Chow, F. Zamborszky, B. Alavi, D. J. Tantillo, A. Baur, C. A. Merlic, and S. E. Brown, Phys. Rev. Lett. **85**, 1698 (2000).
[8] F. Zamborszky, W. Yu, W. Raas, S. E. Brown, B. Alavi, C. A. Merlic, and A. Baur, Phys. Rev. B **66**, 081103(R) (2002).
[9] W. Yu, F. Zhang, F. Zamborszky, B. Alavi, A. Baur, C. A. Merlic, and S. E. Brown, Phys. Rev. B **70**, 121101(R) (2004).
[10] P. Foury-Leylekian, D. LeBolloc'h, B. Hennion, S. Ravy, A. Moradpour, and J.-P. Pouget, Phys. Rev. B **70**, 180405(R) (2004).
[11] T. Takahashi, Y. Nogami, and K. Yakushi, J. Phys. Soc. Jpn. **75**, 051008 (2006).
[12] T. Nakamura, J. Phys. Soc. Jpn. **72**, 213 (2003).
[13] S. Fujiyama and T. Nakamura, Phys. Rev. B **70**, 045102 (2004).
[14] T. Nakamura, K. Furukawa, and T. Hara, J. Phys. Soc. Jpn. **75**, 013707 (2006).
[15] S. Fujiyama and T. Nakamura, J. Phys. Soc. Jpn. **75**, 014705 (2006).
[16] T. Nakamura, K. Furukawa, and T. Hara, J. Phys. Soc. Jpn. **76**, 064715 (2007).
[17] M. Dumm, M. Abaker, M. Dressel, and L. K. Montgomery, J. Phys. IV **131**, 55 (2005); J. Low Temp. Phys. **142**, 609 (2006).
[18] K. C. Ung, S. Mazumdar, and D. Toussaint, Phys. Rev. Lett. **73**, 2603 (1994).
[19] K. Penc and F. Mila, Phys. Rev. B **49**, 9670 (1994).
[20] H. Seo and H. Fukuyama, J. Phys. Soc. Jpn. **66**, 1249 (1997).
[21] S. Mazumdar, S. Ramasesha, R. T. Clay, and D. K. Campbell, Phys. Rev. Lett. **82**, 1522 (1999).
[22] J. Riera and D. Poilblanc, Phys. Rev. B **62**, R16243 (2000).
[23] J. Riera and D. Poilblanc, Phys. Rev. B **63**, 241102(R) (2001).
[24] Y. Shibata, S. Nishimoto, and Y. Ohta, Phys. Rev. B **64**, 235107 (2001).
[25] R. T. Clay, S. Mazumdar, and D. K. Campbell, Phys. Rev. B **67**, 115121 (2003).
[26] H. Seo, J. Merino, H. Yoshioka, and M. Ogata, J. Phys. Soc. Jpn. **75**, 051009 (2006).
[27] T. Ishiguro, K. Yamaji, and G. Saito, *Organic Superconductors* (Springer-Verlag, New York, 1998).
[28] H. Mori, S. Tanaka, and T. Mori, Phys. Rev. B **57**, 12023 (1998).
[29] A. Kawamoto, Y. Honma, and K. I. Kumagai, Phys. Rev. B **70**, 060510(R) (2004).
[30] K. Miyagawa, A. Kawamoto, and K. Kanoda, Phys. Rev. B **62**, R7679 (2000); Phys. Rev. Lett. **89**, 017003 (2002).
[31] B. J. Powell and R. H. McKenzie, J. Phys.: Condens. Matter **18**, R827 (2006).
[32] B. Pedrini J. L. Gavillanos, S. Weyeneth, E. Felder, J. Hinderer, M. Weller, H. R. Ott, V. S. M. Kazakov, and J. Karpinski, Phys. Rev. B **72**, 214407 (2005).
[33] M. Lee, L. Viciu, L. Li, Y. Wang, M. L. Foo, S. Watauchi, R. A. Pascal Jr, R. J. Cava, and N. P. Ong, Nat. Mater. **5**, 537 (2006).
[34] T.-P. Choy, D. Galanakis, and P. Phillips, Phys. Rev. B **75**, 073103 (2007).
[35] S. Lakkis, C. Schlenker, B. K. Chakraverty, R. Buder, and M. Marezio, Phys. Rev. B **14**, 1429 (1976).
[36] M. Isobe and Y. Ueda, J. Phys. Soc. Jpn. **65**, 1178 (1996).
[37] T. Yamauchi, Y. Ueda, and N. Mori, Phys. Rev. Lett. **89**, 057002 (2002).
[38] H. Yoshioka, M. Tsuchiizu, and H. Seo, J. Phys. Soc. Jpn. **75**, 063706 (2006).
[39] H. Seo, Y. Motome, and T. Kato, J. Phys. Soc. Jpn. **76**, 013707 (2007).
[40] We assume equal intermolecular distances along the organic stack. We ignore the intrinsic dimerization that can exist in TMTTF stacks and that can lead to charge localization above T_{CO}.
[41] R. J. J. Visser, S. Oostra, C. Vettier, and J. Voiron, Phys. Rev. B **28**, 2074 (1983).
[42] H. Kobayashi, Y. Ohashi, F. Marumo, and Y. Saito, Acta Crystallogr., Sect. B: Struct. Crystallogr. Cryst. Chem. **26**, 459 (1970).
[43] A. Filhol and M. Thomas, Acta Crystallogr., Sect. B: Struct. Sci. **40**, 44 (1984).
[44] A. Filhol *et al.*, Acta Crystallogr., Sect. B: Struct. Crystallogr. Cryst. Chem. **36**, 2719 (1980).
[45] Y. Nakazawa, A. Sato, M. Seki, K. Saito, K. I. Hiraki, T. Takahashi, K. Kanoda, and M. Sorai, Phys. Rev. B **68**, 085112 (2003).
[46] C. Coulon, G. Lalet, J. P. Pouget, P. Foury-Leylekian, A. Moradpour, and J. M. Fabre, Phys. Rev. B **76**, 085126 (2007).
[47] K. Furukawa, T. Hara, and T. Nakamura, J. Phys. Soc. Jpn. **74**, 3288 (2005).
[48] J.-P. Pouget, P. Foury-Leylekian, D. L. Bolloc'h, B. Hennion, S. Ravy, C. Coulon, V. Cardoso, and A. Moradpour, J. Low Temp. Phys. **142**, 147 (2006).
[49] J. P. Pouget and S. Ravy, Synth. Met. **85**, 1523 (1997).
[50] S. Kagoshima, Y. Saso, M. Maesato, and R. Kondo, Solid State Commun. **110**, 479 (1999).
[51] N. Kobayashi and M. Ogata, J. Phys. Soc. Jpn. **66**, 3356 (1997).
[52] S. Fujiyama and T. Nakamura, J. Phys. Chem. Solids **63**, 1259 (2002).
[53] W. P. Su, J. R. Schrieffer, and A. J. Heeger, Phys. Rev. Lett. **42**, 1698 (1979).
[54] T. Holstein, Ann. Phys. (N.Y.) **8**, 325 (1959).
[55] P. Sengupta, A. W. Sandvik, and D. K. Campbell, Phys. Rev. B **67**, 245103 (2003).
[56] K. Louis and X. Zotos, Phys. Rev. B **72**, 214415 (2005).
[57] M. C. Cross and D. S. Fisher, Phys. Rev. B **19**, 402 (1979).
[58] J. E. Hirsch and D. J. Scalapino, Phys. Rev. B **29**, 5554 (1984).
[59] M. E. Hawley, T. O. Poehler, T. F. Carruthers, A. N. Bloch, D. O. Cowan, and T. J. Kistenmacher, Bull. Am. Phys. Soc. **23**, 424 (1978).
[60] J. B. Torrance, J. J. Mayerle, K. Bechgaard, B. D. Silverman, and Y. Tomkiewicz, Phys. Rev. B **22**, 4960 (1980).
[61] S. N. Dixit and S. Mazumdar, Phys. Rev. B **29**, 1824 (1984).
[62] J. E. Hirsch, Phys. Rev. Lett. **53**, 2327 (1984).
[63] S. Mazumdar, R. T. Clay, and D. K. Campbell, Phys. Rev. B **62**, 13400 (2000).
[64] E. Sorensen, I. Affleck, D. Augier, and D. Poilblanc, Phys. Rev. B **58**, R14701 (1998).
[65] W. Yu and S. Haas, Phys. Rev. B **62**, 344 (2000).
[66] O. F. Syljuasen and A. W. Sandvik, Phys. Rev. E **66**, 046701

(2002).
[67] R. P. Hardikar and R. T. Clay, Phys. Rev. B **75**, 245103 (2007).
[68] E. H. Lieb and D. Mattis, J. Math. Phys. **3**, 749 (1962).
[69] J. Voit, Rep. Prog. Phys. **58**, 977 (1995).
[70] R. T. Clay, A. W. Sandvik, and D. K. Campbell, Phys. Rev. B **59**, 4665 (1999).
[71] J. E. Hirsch and E. Fradkin, Phys. Rev. B **27**, 4302 (1983).
[72] M. Kuwabara, H. Seo, and M. Ogata, J. Phys. Soc. Jpn. **72**, 225 (2003).
[73] R. T. Clay, S. Mazumdar, and D. K. Campbell, Phys. Rev. Lett. **86**, 4084 (2001).
[74] D. Graf, E. S. Choi, J. S. Brooks, R. T. Henriques, M. Almeida, and M. Matos, Phys. Rev. Lett. **93**, 076406 (2004).
[75] R. D. McDonald, N. Harrison, L. Balicas, K. H. Kim, J. Singleton, and X. Chi, Phys. Rev. Lett. **93**, 076405 (2004).